Drug Delivery and Translational Research (2022) 12:3029–3046
https://doi.org/10.1007/s13346-022-01168-9

ORIGINAL ARTICLE

Amalgamation of solid dispersion and melt adsorption techniques for augmentation of oral bioavailability of novel anticoagulant rivaroxaban

Pranav J. Shah[1] · Milan P. Patel[1] · Jigar Shah[2] · Anroop B. Nair[3] · Sabna Kotta[4] · Bhavin Vyas[1]

Accepted: 15 April 2022 / Published online: 25 April 2022

Abstract

The objective of the present study was to evaluate the potential of solid dispersion adsorbate (SDA) to improve the solubility and bioavailability of rivaroxaban (RXN). SDA of RXN was developed by fusion method using PEG 4000 as carrier and Neusilin as adsorbent. A 3^2 full factorial design was utilized to formulate various SDAs. The selected independent variables were the amount of carrier (X_1) and amount of adsorbent (X_2). The responses measured were the time required for 85% drug release (Y_1) and saturated solubility (Y_2). MTT assay was employed for cytotoxicity studies on Caco-2 cells. In vivo pharmacokinetics and pharmacodynamic evaluations were carried out to assess the prepared SDA. Pre-compression evaluation of SDA suggests the prepared batches (B1–B9) possess adequate flow properties and could be used for compression of tablets. Differential scanning calorimetry and X-ray diffraction data signified the conversion of the crystalline form of drug to amorphous form, a key parameter accountable for improvement in drug dissolution. Optimization data suggests that the amount of carrier and amount of adsorbent significantly ($P < 0.05$) influence both dependent variables. Post-compression data signifies that the compressibility behavior of prepared tablets was within the official standard limits. A significant increase ($P < 0.0001$) in the in vitro dissolution characteristics of RXN was noticed in optimized SDA (> 85% in 10 min) as compared to the pure drug, marketed product, and directly compressible tablet. Cytotoxicity studies confirmed the nontoxicity of prepared RXN SDA tablets. RXN SDA tablets exhibited 2.79- and 1.85-fold higher AUC in comparison to RXN suspension and Xarelto tablets respectively indicating improved oral bioavailability. Higher bleeding time and percentage of platelet aggregation noticed with RXN SDA tablets in comparison to RXN suspension further substantiate the efficacy of the prepared formulation. In summary, the results showed the potential of RXN SDA tablets to enhance the bioavailability of RXN and hence can be an alternate approach of solid dosage form for its development for commercial application.

Keywords Rivaroxaban · Solid dispersion adsorbate · Dissolution · Factorial design · Pharmacokinetics · Pharmacodynamics

Introduction

For decades, vitamin K antagonists (VKAs) are the only therapeutic category of orally administered anticoagulants. However, VKAs have been associated with demerits including numerous drug-drug and food-drug interactions, a large intra- and inter-individual variation of their dose–response relationship, slow onset and offset of action, and an unpredictable pharmacodynamic response that mandates routine coagulation monitoring and dose adjustment. In recent years, direct oral anticoagulants that are specific in targeting a single coagulation factor (such as Factor Xa or thrombin) have been developed to surpass the limits of VKAs. Rivaroxaban (RXN) is a direct, specific Factor Xa inhibitor that has been

✉ Pranav J. Shah
pranav.shah@utu.ac.in

[1] Maliba Pharmacy College, Uka Tarsadia University, Bardoli, Surat 394350, India

[2] Department of Pharmaceutics, Institute of Pharmacy, Nirma University, Ahmedabad 382481, India

[3] Department of Pharmaceutical Sciences, College of Clinical Pharmacy, King Faisal University, Al-Ahsa 31982, Saudi Arabia

[4] Department of Pharmaceutics, Faculty of Pharmacy, King Abdulaziz University, Jeddah 21589, Saudi Arabia

approved for clinical use in 2008 to prevent venous thromboembolism in adults undergoing elective hip or knee replacement surgery. It has also been employed for the prevention of stroke, systemic embolism, and atherothrombotic events along with prevention and treatment of deep vein thrombosis and pulmonary embolism. RXN is associated with merits of rapid onset of action, limited drug-drug interactions, well-established pharmacokinetics, and pharmacodynamics, does not require routine coagulation monitoring, making it a potential anticoagulant in simplifying and improving the management of thromboembolic disorders [1, 2]. However, RXN is lipophilic, non-ionizable, and, practically insoluble in water with pH-independent solubility of 5–7 mg/L at 25 °C [3].

Numerous novel formulation strategies have been utilized to enhance the aqueous solubility of BCS class II drugs, like liposomes, cyclodextrin inclusion complexes, use of cosolvents, nanoemulsion, nanosuspensions, solid dispersions, etc. [4–8]. Various studies have been done for enhancing the solubility, dissolution characteristics, and bioavailability of RXN including inclusion complexes [9], self-nanoemulsifying drug delivery systems (SNEDDS) [2, 3], nanoparticles [4], and microparticles [10]. However, these formulation strategies are not devoid of limitations, and scaling up in industries is a major challenge.

Solid dispersion consists of a minimum of two different components, usually a hydrophilic inert carrier/matrix and a lipophilic drug. The carrier may be amorphous or crystalline. Typically, it is a dispersion of an active ingredient in a matrix or in an inert carrier formulated by melting, using solvent, or melting solvent method. In this system, the drug experiences particle size reduction, and as a result, dissolution is increased due to an increase in surface area. Additionally, no energy is needed to break the crystal lattice of the drug in the amorphous state throughout the dissolution step [11]. Due to the presence of surrounding hydrophilic carriers, drug wettability, as well as solubility, will be increased further [12]. Attempts were also made to formulate solid dispersions of RXN to enhance the drug dissolution and solubility and thereby enhance the absorption [13–15]. However, there are some limitations to this technique as well, which include difficulty in grinding, inadequate flow, poor compressibility, and also less reproducibility of physicochemical properties and instability of the drug and vehicle as well as difficulty in scale-up [5, 16]. The concept of solid dispersion adsorbate (SDA) was introduced to control these problems. In this method, solid dispersion is adsorbed on a carrier with a very large surface area to obtain a free-flowing powder and thereby help in an increase in dissolution as well as bioavailability [17–19]. There are a variety of commercially available porous carriers like Florite, Neusilin US2, Aerosil, Aerogel, etc. having unique characteristics like pore size, particle size, specific surface area, etc., and have been widely investigated in tablet formulations [20–22]. Neusilin US2 is amorphous aluminum magnesium silicate with a high level of specific surface area and good adsorption capacity. On the other hand, polyethylene glycol (PEG) has been widely used in various oral formulations including tablets, microcapsules, soft gelatin capsules, suspensions, and emulsions [23]. Indeed, PEG 4000 (hydrophilic polymer) is one of the most widely studied polymeric carriers in preparing solid dispersion [24–26]. Various research groups have emphasized the influence of carrier and adsorbent on the solubility and dissolution of SDAs [17–19]. A review of the literature suggests that no work has been done to date on formulating RXN SDA for solubility enhancement. The objective of this study was to formulate SDAs of BCS class II drug-RXN by the amalgamation of solid dispersion and melt adsorption techniques and assess its potential to improve solubility and dissolution. Amounts of PEG 4000 and Neusilin US2 were the critical material attributes that could affect quality attributes such as dissolution and solubility. A 2-factor, 3-level experimental design was employed for statistical optimization, wherein the impact of independent variables [amount of PEG 4000 (X_1) and amount of Neusilin US2 (X_2) on the dependent variables [time required for 85% drug release (Y_1) and saturated solubility (Y_2) was assessed. The prepared SDA batches (B1-B9) were assessed for both pre and post-compression properties. Optimized RXN SDA was evaluated for cytotoxicity, pharmacokinetics, and pharmacodynamics properties.

Materials and methods

Materials

RXN was obtained from Symed Labs limited, Hyderabad, India. Neusilin US2 was obtained from Gangwal Chemicals Pvt. Ltd., Mumbai, India. Microcrystalline cellulose (Avicel PH 102) was purchased from Signet, Mumbai, India. Polyethylene glycol (PEG) 4000, crospovidone, magnesium stearate, and talc were acquired from S.D. Fine Chem. Products, Mumbai, India. The cell lines of human colorectal adenocarcinoma (Caco-2) were procured from the National Center for Cell Science, Pune, India. Culturing of cells was performed in Dulbecco's Modified Eagle's medium (Sigma-Aldrich, USA) supplemented with 10% fetal bovine serum, 100 IU/mL penicillin, 100 µg/mL streptomycin, and 1% non-essential amino acids in a humidified environment of 5% CO_2 using a carbon dioxide incubator (Thermo Scientific, Waltham, MA, USA) at 37 °C. Xarelto® tablets 10 mg (BAYER, Germany) were purchased from a medical store. All other chemicals were of analytical grade.

Preparation of RXN SDA

SDA of RXN was prepared by a fusion method reported in the literature [17] with minor modifications. In this method, RXN was sifted through sieve number 100. The carrier (PEG 4000) was melted in a porcelain dish and heated till its melting point (57–63 °C) on a hot plate. Then, RXN (0.435 g) was dispersed into melted carrier mass with constant stirring to form solid dispersion. Further, the adsorbent (Neusilin US2) was added and stirred until the blend is converted into a free-flowing powder. The SDA was then passed through sieve number 40.

Experimental design (QBD-DoE approach)

A 2-factor, 3-level full factorial experimental design was chosen to optimize various formulation parameters statistically and the effects of various formulation components on solubility and in vitro release of formulations were evaluated. The selected dependent and independent variables are presented in Table 1 along with their low (− 1), medium (0), and high (+ 1) levels. The amounts of carrier and adsorbent were selected from the results of preliminary experiments and previous literature [27, 28]. An experimental design comprising 9 design batches was developed with different amounts of the carrier (X_1) and amount of adsorbent (X_2) coded and non-coded values of design batches are shown in Table 2.

Percentage yield and solubility

Percentage yields of the prepared SDA batches (B1–B9) were calculated using the following equation;

$$\%\ Practical\ yield = \frac{(\text{weight of prepared SDA})}{\text{Theoretical weight of SDA}} * 100 \quad (1)$$

Table 1 Independent and dependent variables used for experimental design

	Levels		
	Low (− 1)	Medium (0)	High (+ 1)
Independent variables			
Amount of carrier; PEG 4000 (g) = X_1	4	6	8
Amount of adsorbent; Neusilin US2 (g) = X_2	0	1.5	3
Dependent variables			
$Y_1 = t_{85\%}$ (time required for 85% drug release)			
Y_2 = saturated solubility(g/mL)			

Table 2 Formulation of RXN SDA batches

Batch no	X_1	X_2	Polyethylene glycol 4000 (g)	Neusilin US2 (g)
B1	− 1	− 1	4	0
B2	− 1	0	4	1.5
B3	− 1	+ 1	4	3
B4	0	− 1	6	0
B5	0	0	6	1.5
B6	0	+ 1	6	3
B7	+ 1	− 1	8	0
B8	+ 1	0	8	1.5
B9	+ 1	+ 1	8	3

Saturation solubility

The solubility of the RXN in prepared SDA batches (B1–B9) was estimated by adding an excess amount of drug-containing SDAs in 10 mL of distilled water in glass vials [29]. The mixture was mixed in a thermomixer C (MixMate, Eppendorf, Germany). The shaking of the mixture continued for 24 h at 25 °C. The solution was then sonicated for 20 min and the supernatant was taken and passed through a syringe filter (0.45 µm). The filtrate was diluted and the absorbance was recorded on a UV spectrophotometer (UV Shimadzu 1800 Scientific Instrument, Japan) at λ_{max} of 248 nm. A similar procedure was appointed to determine the solubility of pure drug-RXN and the value was employed as control.

Pre-compression evaluation

The angle of repose, bulk density, tapped density, Carr's index, and Hausner's ratio of prepared RXN-SDA blends were measured using standard protocols. The pre-compression parameters were also determined for pure drug-RXN and the values were employed as control [30, 31].

Formulation of RXN SDA tablets

Table 3 shows the composition of tablets prepared from RXN SDA. SDA equivalent to 10 mg of RXN was taken followed by the addition of Avicel PH 102 and crospovidone and mixing for 5 min. Then magnesium stearate and talc were sifted through sieve number 100, added to the above blend, and mixed for 2 min. The lubricated blend was compressed into tablets using a 10-mm punch in a tablet compression machine (Rimek mini press-I, Ahmedabad, India). A compression force of 10 kN was applied.

Table 3 Composition of immediate release SDA tablets

Batch no	Solid dispersion adsorbate (mg)*	Crospovidone (mg)	Micro crystalline cellulose (mg)	Talc (mg)	Magnesium stearate (mg)	Quantity per tablet (mg)
B1	101	15	179	2.5	2.5	300
B2	136	15	144	2.5	2.5	300
B3	170	15	110	2.5	2.5	300
B4	147	15	133	2.5	2.5	300
B5	182	15	98	2.5	2.5	300
B6	216	15	64	2.5	2.5	300
B7	193	15	87	2.5	2.5	300
B8	228	15	52	2.5	2.5	300
B9	262	15	18	2.5	2.5	300

*Equivalent to 10 mg of RXN

Formulation of directly compressible tablets

The directly compressible tablets were prepared by simple mixing of RXN (10 mg; sifted through sieve number 100), PEG 4000 (142 mg), Neusilin US2 (64 mg), crospovidone (15 mg), and Avicel PH 102 (64 mg) for 5 min. Then, magnesium stearate (2.5 mg) and talc (2.5 mg) were sifted through sieve number 100, added to the above blend, and mixed for 2 min. The lubricated blend was compressed into tablets using a 10-mm punch in tablet compression machine (Rimek mini press-I, Ahmedabad, India). A compression force of 10 kN was applied.

Post-compression evaluation of RXN SDA tablets

The compressed tablets were characterized for general appearance, thickness, weight variation, hardness, friability, disintegration time, and assay according to the standard protocols [32].

Drug content

Ten tablets were weighed and finely powdered using a mortar. An amount of the powdered mass equivalent to 10 mg of RXN was accurately weighed and transferred to a 100 mL volumetric flask. Acetonitrile: water (1:1, 50 mL) was added, and the mixture was sonicated for 15 min to ensure complete extraction of RXN followed by volume make up with acetonitrile: water (1:1). The solution was filtered through a 0.45-µm membrane filter and analyzed spectrophotometrically at 249 nm [33].

In vitro dissolution

The dissolution profile of immediate-release tablets prepared from the SDA batches (B1-B9) was done on USP type II apparatus (Electrolab TDT-08L, Mumbai, India) at 75 rpm. The dissolution medium used was acetate buffer (pH 4.5; 900 mL) containing 0.4% sodium dodecyl sulfate with a temperature setting at 37 ± 0.5 °C [34]. Samples (5 mL) were withdrawn for analysis at different time points (5, 10, 15, 20, 25, 30, 40, 50, and 60 min). The withdrawn volume of the sample from the dissolution vessel was replenished every time with an equal volume of the dissolution media to maintain sink conditions. The sample was analyzed at 248 nm using UV spectroscopy after filtering through a Millipore filter (0.45 µm; Spectrum Medical Inc., San Diego, CA). Using the calibration curve equation, the cumulative percentage of RXN release at various time intervals was calculated. Similarly, in vitro drug release of optimized SDA tablet was performed and the profiles were compared with RXN suspension (*Z*-average: 989.8 nm; PDI: 1.0), marketed product (Xarelto® 10-mg tablets), and directly compressible tablets.

Generation of polynomial equations and response surface plots

Through the use of the Design-Expert software, polynomial equations and 3D graphs were generated to assess the correlation between independent and dependent variables. Analysis of variance (ANOVA) was employed to assess the significance of the independent variables on the responses [35].

Constrained and graphical optimization of RXN-SDAs

To select the most appropriate formulation, a numerical optimization technique based on the desirability function was employed [36]. The constraints laid down at the start of the experiment on the responses of RXN-SDAs included (i) t_{85} (Y_1): lowest and (ii) saturated solubility (Y_2): highest. The solutions provided by the Design-Expert software were

sorted in the descending order of their desirability values and the formulation with the highest desirability factor (values close to 1) was considered for optimization. Graphical optimization was also performed by applying constraints to generate design space [37].

Validation of experimental design

A 3^2 factorial design, employed for the formulating RXN-SDAs, was validated by preparing a checkpoint batch. Based on the values of independent variables obtained from the desirability function and overlay plot, an optimized batch of RXN-SDAs was formulated. Comparisons of the experimental and predicted values of the responses were performed to confirm the validity of the design [37].

Evaluation of optimized RXN SDA (pre-compression)

Compressibility and flowability

The angle of repose, bulk density, tapped density, Carr's index, and Hausner's ratio of optimized RXN-SDA blend was determined by the procedure described above [30, 31].

FTIR spectroscopy

The IR peaks of optimized SDA, RXN, and Neusilin US2 were characterized by FTIR spectroscopy (Bruker Optics GmbH, Ettlingen, Germany). RXN and potassium bromide were mixed and made into pellets by compressing the powder mixture on a potassium bromide press at 20 psi for 10 min [38]. The spectrum was taken from the range of 4000 to 400 cm^{-1} (Wavenumber).

X-ray powder diffraction

Diffractograms of RXN, Neusilin US2, and SDA were recorded using a diffractometer (Rigaku Corporation-Miniflex, Surat, India). The samples were finely ground in a mortar with the help of a pestle and samples were irradiated with X-ray at a scanning angle in the range of 0 to 40° of 2θ.

Differential scanning calorimetry

DSC thermograms of RXN, Neusilin US2, and SDA were characterized by DSC (DSC-60, Shimadzu Corporation, Kyoto, Japan). The thermal performance of the samples was studied by keeping (3–5 mg) in an aluminum pan and sealing hermetically, while a blank pan was used as standard reference [39]. Thermal behavior was determined at a scanning speed of 10 °C/min at a temperature between 25 and 300 °C under a nitrogen atmosphere (10 mL/min).

Surface morphology

Morphological examination of prepared SDA was carried out by scanning electron microscopy (Hitachi S-3400, India) operated at a specific voltage of 15 kV. Samples were mounted on metal stubs and were made conductive by coating with platinum in neutral condition while maintaining the pressure [40]. Then, the images were captured using a microscope.

Evaluation of optimized SDA (post-compression)

The weight variation, thickness, hardness, friability, drug content, disintegration time, and in vitro dissolution of the optimized RXN SDA tablets were performed as per the procedures mentioned above.

Cytotoxicity test

The cytotoxicity of prepared RXN SDA tablets and suspension containing RXN against the Caco-2 cell line was determined by MTT assay. In brief, cells were seeded at a density of 7.5×10^4 cells/mL (200 µL/well) in 96-well culture plates and incubated with 20–100 µM of RXN SDA tablets or RXN suspension. After 24 h of incubation, the MTT reagent (25 µL; 5 mg/mL in PBS, 25 µL/well) was poured into the individual well and kept at 37 °C for 4 h, to metabolize MTT. The formed formazan precipitate was dissolved by adding DMSO (100 µL) to every well. The optical density of the samples was determined at 570 nm with the help of a plate reader (Bio-Rad, iMark, Hercules, CA, USA) and the background was deducted at 630 nm. The estimation of percent cell viability was made based on the formula described in the literature [41].

Pharmacokinetic study

A total of 18 male Sprague–Dawley rats were included in the study. The animals were randomly divided into three groups. Group I, group II, and group III were administered RXN suspension, RXN SDA tablets, and Xarelto tablets respectively (equivalent to 10 mg/kg of RXN) [42]. RXN SDA tablets and Xarelto tablets were powdered and dispersed in 0.5% w/v carboxymethyl cellulose [43]. The study was performed in Maliba Pharmacy College, Uka Tarsadia University, as per the animal ethics committee approved protocol MPC/IAEC/21/2017 and CPCSEA guidelines. Each group was administered 0.5 mL of the sample by oral route. At particular time intervals (0, 0.25, 0.5, 1, 2, 3, 4, 8, 12, and 24 h), 200 µL of blood was collected from the post-orbital plexus. Blood samples were centrifuged for 5 min at 4 °C in a cooling centrifuge at 16,000 × g, and the supernatant plasma was collected. The WinNonlin software 8.1

(Pharsight, Sunnyvale, CA, USA) was employed to perform non-compartmental pharmacokinetic analysis. From the plot of drug plasma level vs. time, pharmacokinetic parameters, namely maximum plasma concentration of RXN (C_{max}) and the time required to achieve the maximum plasma concentration of RXN (T_{max}) were calculated. The area under the curve (AUC) was determined using the trapezoidal law from 0 to 24 h (AUC_{0-24}), and extrapolating the time to infinity was used to calculate the AUC of the profile from 0 to infinite time ($AUC_{0-\infty}$).

Estimation of RXN in plasma

Chromatographic analysis of rivaroxaban was carried out on an HPLC–DAD system consisting of Shimadzu LC-2010-CHT equipped with a binary pump (LC20AT), injection (Rheodyne, 20µL loop), and photodiode array detector (SPD-M20A). The data was captured using LC solution software Ver. 1.25 (Shimadzu, Japan). The wavelength of the detector was set at 249 nm. The chromatographic separation was achieved using a reverse-phase octadecyl silane C 18 (250 mm × 4.6 mm; 5 µm) (GraceSmart) column. The mobile phase consisting of a 90:10 v/v mixture of (A) water containing 0.1% of formic acid and (B) acetonitrile was isocratically pumped at 1 mL/min. The injection volume was 20 µL [44]. All determinations were performed at 25 °C.

Pharmacodynamic studies

Pharmacodynamic studies were performed in Maliba Pharmacy College, Uka Tarsadia University, as per the animal ethics committee approved protocol MPC/IAEC/21/2017 and CPCSEA guidelines.

Tail bleeding time assay

Animals were divided into three groups comprising 6 rats per group, to estimate tail bleeding duration. Group I received 0.5% w/v carboxymethyl cellulose (control); group II received RXN suspension and group III received RXN SDA tablets dispersed in 0.5% carboxymethyl cellulose. Groups II and III received doses equivalent to 10 mg/kg of RXN. All treatments were given orally once. Four hours post-administration; animals were anesthetized by administering pentobarbital sodium (50 mg/kg intraperitoneal) [45]. The method of Wang et al. (2004) with slight modifications was adopted to determine the rat tail bleeding time [46]. A 5-mm rat tail tip was amputated with a scalpel to determine the bleeding time, and blood was blotted onto filter paper every 30 s before the staining of the paper with blood ceased. The bleeding time was described as the time between the amputation of the tail and the cessation of bleeding (min).

Platelet aggregation

This study was performed in rats for all three groups after the tail bleeding time assay. Blood was spontaneously withdrawn from the abdominal aorta and collected in the vial containing anticoagulant, acid-citrate-dextrose (9:1, v/v containing citric acid 130 mM, trisodium citrate 170 mM, dextrose 4%). The platelets were prepared according to the process mentioned previously [47]. Briefly, platelet-rich plasma was collected by centrifuging blood at 3600 rpm for 15 min. In vitro platelet aggregation was evaluated according to the method of Born [48]. Platelet aggregation was performed using an aggregometer at 37 ºC and 1000 rpm. The 240-µL washed platelets were stimulated with an aggregating agent, i.e., collagen (5 mg/mL). Platelet aggregation was registered for a 10-min period after platelet stimulation.

Data analysis

The statistical interpretation of experimental data was carried out with GraphPad Prism (version 6, GraphPad, San Diego, CA, USA). The difference in values at $P < 0.05$ is considered statistically significant.

Results and discussion

Flow characteristics of SDA

RXN-SDA blends (B1–B9) were evaluated for angle of repose, Carr's index, and Hausner's ratio, and the results are presented in Table 4. The angle of repose, Carr's index, and Hausner's ratio were found in the range of 17.25–27.78°; 9.25–22.78%, and 1.09–1.22 respectively indicating fair flow properties, which is a prerequisite for commercial manufacturing. Neusilin US2 possesses a large surface area and porous nature and has been widely employed for flow improvement. The adsorption of RXN solid dispersions onto Neusilin US2 contributed to improved flowability and compressibility of solid dispersions, which otherwise are known to be sticky.

Percentage yield

The percentage yields of RXN-SDA batches (B1–B9) were found in the range of 95–98% (Table 5). The high values for percentage yield were indicative of the minimum loss, homogeneity, and accuracy of the process, and hence the suitability for scale-up.

Table 4 Flow characteristics of RXN SDA batches

Batch no	Angle of repose (°)	Bulk density (g/cm^3)	Tapped density (g/cm^3)	Carr's index (%)	Hausner's ratio
B1	27.78 ± 0.16	0.68 ± 0.05	0.79 ± 0.07	13.85 ± 1.03	1.15 ± 0.01
B2	21.64 ± 0.11	0.43 ± 0.02	0.53 ± 0.03	18.12 ± 0.10	1.21 ± 0.01
B3	17.25 ± 0.29	0.42 ± 0.02	0.46 ± 0.03	9.25 ± 0.65	1.09 ± 0.01
B4	20.92 ± 0.11	0.53 ± 0.03	0.59 ± 0.04	10.82 ± 0.80	1.11 ± 0.01
B5	20.41 ± 0.21	0.46 ± 0.03	0.51 ± 0.03	9.96 ± 0.58	1.10 ± 0.01
B6	17.73 ± 0.31	0.43 ± 0.02	0.51 ± 0.05	9.62 ± 0.65	1.17 ± 0.08
B7	22.07 ± 0.24	0.79 ± 0.07	0.94 ± 0.09	16.15 ± 1.47	1.18 ± 0.02
B8	21.40 ± 0.18	0.57 ± 0.04	0.75 ± 0.07	22.78 ± 0.44	1.22 ± 0.11
B9	18.10 ± 0.14	0.43 ± 0.02	0.50 ± 0.05	9.62 ± 0.64	1.11 ± 0.07

Saturated solubility

The aqueous solubility of pure RXN was found to be 0.012 ± 0.009 g/mL whereas the values for batches B1-B9 were found in the range of 0.023–0.041 g/mL. The highest RXN solubility noticed was 0.041 mg/mL, which is 3.4 times higher as compared to the solubility of pure RXN. This improvement in solubility of RXN could be due to PEG 4000 (hydrophilic carrier) that improves the wettability of the drug [49] as well as Neusilin US2 (adsorbent), which increases the surface area of the formulation [50, 51].

FTIR

The FTIR spectra of pure RXN, PEG 4000, Neusilin US2, and SDA are presented in Fig. 1. The prominent peaks of various functional groups of RXN were observed at 3351 cm^{-1} (N–H stretch), 1736 cm^{-1} (C = O stretch carbonyl group), 1646 cm^{-1} (C = O stretch ester group), 1516 cm^{-1} (N–O stretch), and 828 cm^{-1} (Benzene stretch). From the figure, it is observed that the infrared spectrum of pure drug and SDA have a significant difference in the absorption peak intensity, probably due to the low concentration of drug compared to the excipients used. A slight shift towards the lower wavelength or broadening was noticed in a few peaks. These subtle changes could be attributed to the intermolecular hydrogen bonding and/or van der Waals interactions between RXN and PEG 6000. Hydrogen bonds are essential in solid dispersions because they reduce molecular mobility, depress the driving force of crystallization, and thus enhance the stability and solubility of the solid dispersion compared to pure RXN. A similar finding has been reported by another research group [52].

XRD

The diffraction spectra of RXN, PEG 4000, Neusilin US2, and RXN SDA are shown in Fig. 2. The graph of pure RXN showed the high crystalline nature of the drug with main diffraction peaks. The X-ray diffractogram of SDA did not show any characteristic peaks which are observed in pure drug diffraction patterns, which indicates the transformation of crystalline to an amorphous form of the drug. The possible reason for this change could be due to the annihilation of RXN crystal lattice, because of homogenous dispersion of drugs into molten carriers. Therefore, the reduction in crystallinity of the drug might be causing improvement in the dissolution of RXN [53].

Table 5 Evaluation of physicochemical properties of immediate release SDA tablets

Batch no	% yield	Average weight (mg)	Thickness (mm)	Hardness (kg/cm^2)	% Friability	Disintegration time (s)	Drug content (%)
B1	95.83 ± 1.02	302 ± 4.02	3.10 ± 0.02	2.83 ± 0.28	0.48 ± 0.05	44.23 ± 1.52	101.12 ± 1.62
B2	96.03 ± 1.68	301 ± 4.24	3.43 ± 0.01	2.60 ± 0.17	0.53 ± 0.04	34.33 ± 0.57	102.35 ± 1.45
B3	95.84 ± 0.86	301 ± 4.10	3.33 ± 0.01	2.50 ± 0.26	0.58 ± 0.01	26.00 ± 2.64	100.52 ± 1.04
B4	95.84 ± 0.23	303 ± 3.74	3.48 ± 0.02	2.70 ± 0.20	0.46 ± 0.02	41.33 ± 1.52	102.45 ± 1.24
B5	97.45 ± 1.45	302 ± 3.19	3.31 ± 0.01	2.55 ± 0.14	0.40 ± 0.01	29.33 ± 2.08	104.12 ± 0.65
B6	96.90 ± 0.54	300 ± 2.97	3.44 ± 0.01	2.41 ± 0.20	0.32 ± 0.02	25.33 ± 0.57	103.14 ± 1.68
B7	96.83 ± 0.49	303 ± 3.27	3.19 ± 0.01	2.73 ± 0.12	0.45 ± 0.03	43.66 ± 2.08	104.68 ± 0.63
B8	97.54 ± 1.05	302 ± 3.34	3.41 ± 0.01	2.63 ± 0.20	0.34 ± 0.04	31.00 ± 2.64	105.12 ± 1.64
B9	98.23 ± 0.36	300 ± 2.70	3.14 ± 0.01	2.56 ± 0.21	0.32 ± 0.02	27.66 ± 0.57	104.26 ± 1.38

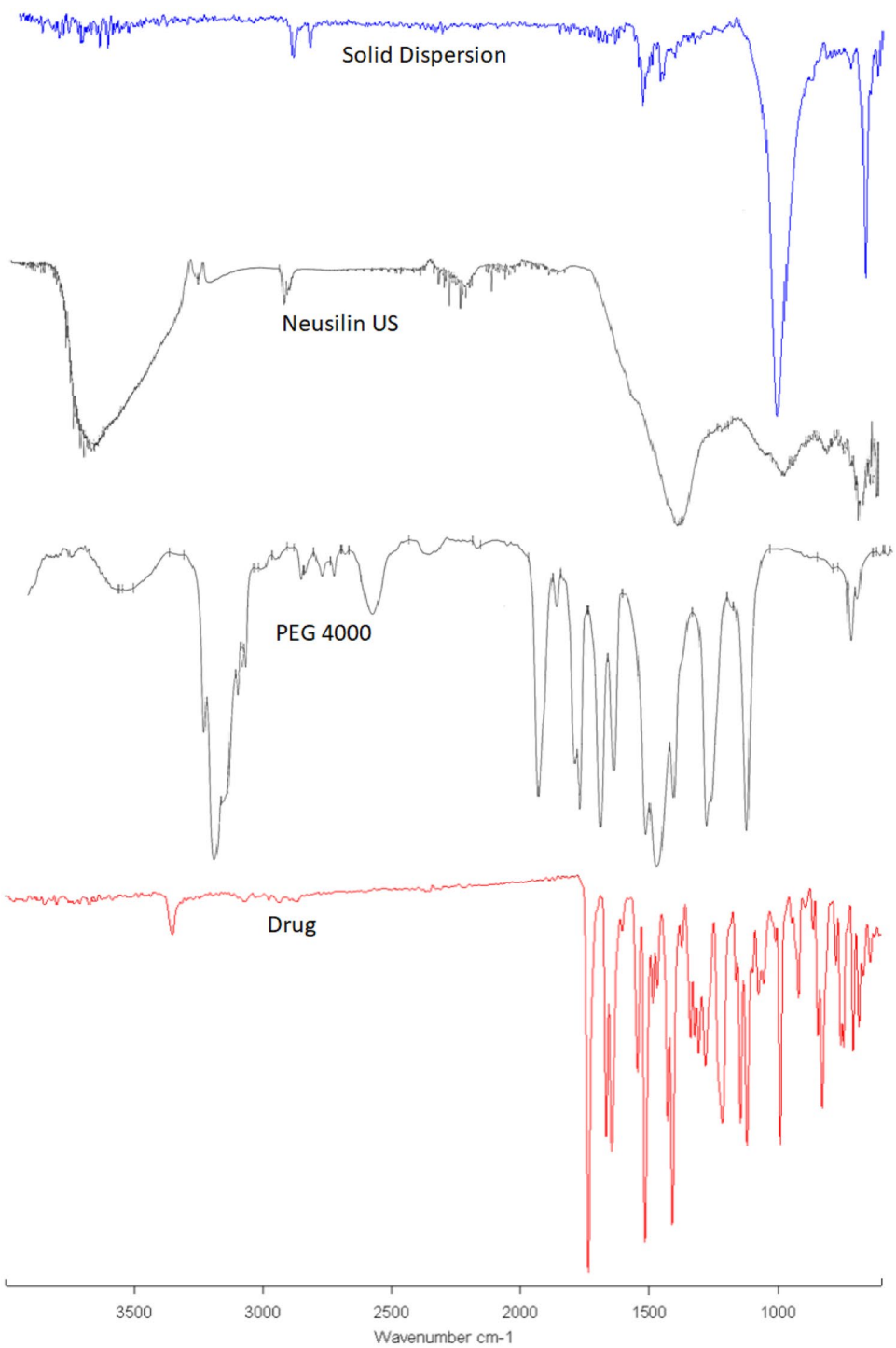

Fig. 1 FTIR spectra of pure rivaroxaban, polyethylene glycol 4000, Neusilin US2, and RXN SDA

DSC

The DSC thermogram of a pure drug, Neusilin US2, PEG 4000, and SDA are presented in Fig. 3. RXN showed a distinct strong endothermic peak at 230 °C (which is the drug melting point), which indicates its crystalline nature. However, the DSC of SDA did not show any peak of pure RXN; this might be due to the complete dissolution of RXN in the melted polymer which indicated that the drug can be in an amorphous state [54].

Surface morphology

SEM images were captured to observe the surface morphology of the SDA (Fig. 4). The SEM image of the RXN powder exhibited its crystalline nature and irregular shape. The

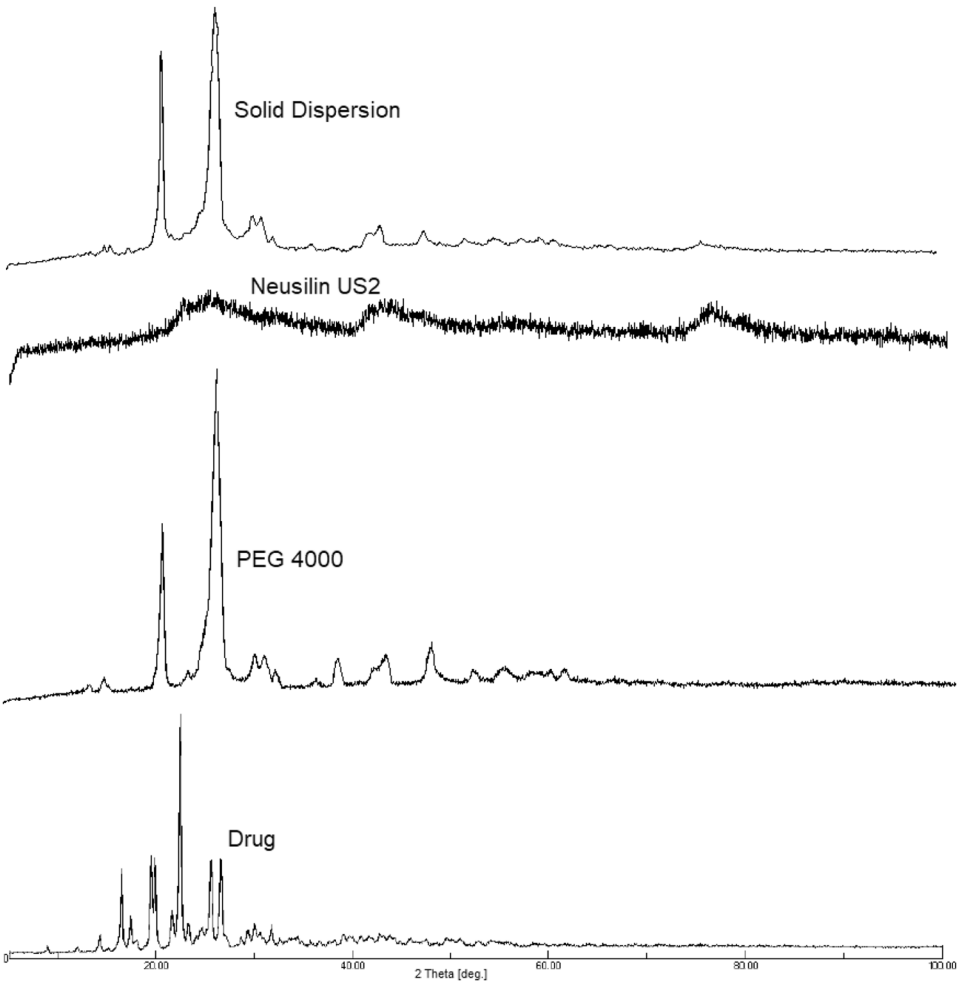

Fig. 2 X-ray diffractogram of pure rivaroxaban, polyethylene glycol 4000, Neusilin US2, and RXN SDA

SEM of RXN SDAs exhibited the disappearance of RXN crystals and a spherical shape. The disappearance of RXN crystals could be attributed to the molecular dispersion of RXN in PEG 4000. The spherical shape and non-aggregated particles of RXN SDAs due to adsorption on Neusilin US2 would provide good flowability and compressibility to RXN SDAs, which otherwise have a sticky nature [55].

Post-compression characterization of SDA tablets

Physical examination of tablets from each batch showed that all the tablets were circular, white to off white, flat, and without any physical defects. The thickness of SDA tablets ranged from 3.10 ± 0.02 to 3.48 ± 0.02 mm (Table 5) while the diameter of tablets was found to be in the range of 8.10 ± 0.001 to 8.19 ± 0.001 mm, hence all tables are in the acceptable range. Similarly, all formulations showed uniformity of weight within the pharmacopeia limits for uncoated tablets. The hardness of SDA tablets ranged from 2.41 ± 0.20 to 2.83 ± 0.28 kg/cm^2 (Table 5), which assures the ability of the tablets to withstand wear and tear during handling and transportation. Friability was in the range of 0.32 ± 0.02 to 0.48 ± 0.05% (Table 5), which ensures acceptable resistance by tablets to withstand mechanical shocks. Disintegration time ranged between 25.33 ± 0.57 to 44.23 ± 1.52 s (Table 5). The percentage drug contents of all the batches of SDA were found in the range of 96.15–99.60%, indicating the uniformity of the drug in the developed formulation. All the post-compression parameters were satisfactory suggesting that the developed formulation can be scaled up with success.

Fitting data to the model

A 2-factor, 3-level experimental design was utilized as the RSM needed 9 experiments. The responses observed with all the nine batches were concurrently fit to a quadratic model using design expert software version 11.0. The independent variables and responses of dependent variables are shown in Table 6. A positive number indicates an effect that favors the optimization, on the other hand, a minus number suggests that the relationship between factor and response is negative.

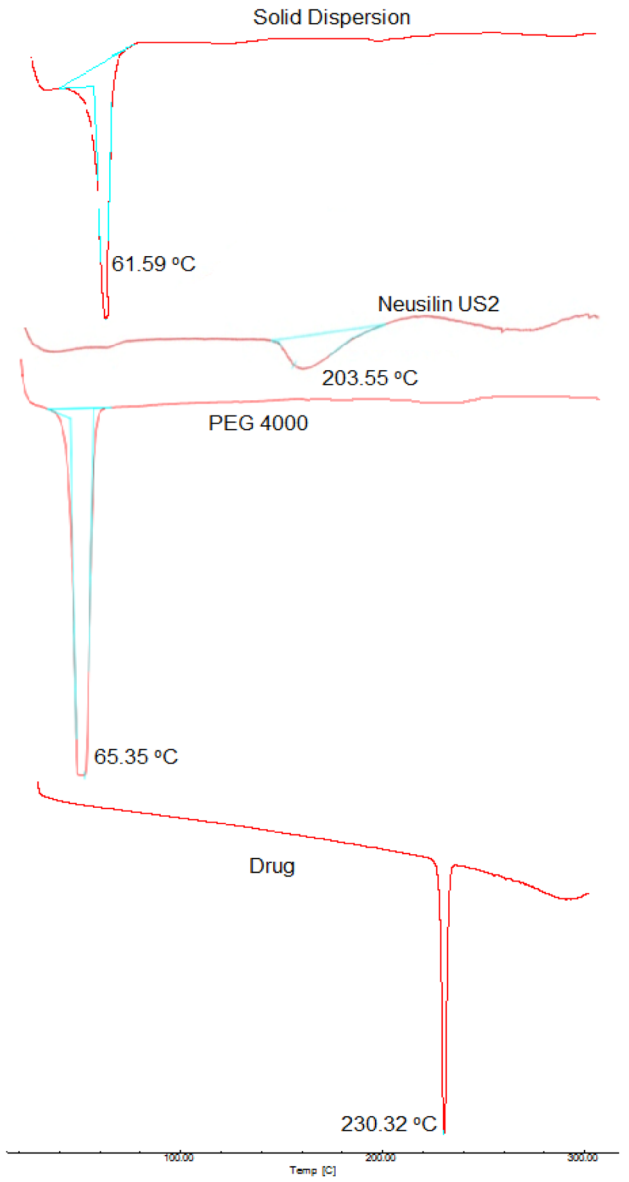

Fig. 3 DSC thermograms of RXN, PEG 4000, Neusilin US2 and RXN SDA

It is evident that both the independent variables, viz., the amount of carrier (X_1) and the amount of adsorbent (X_2) have positive effects on the responses, viz., t_{85} (time required for 85% drug release) and saturated solubility (g/mL).

Effect of amount of PEG 4000 (X_1) and amount of Neusilin US2 (X_2) on time required for 85% drug release (Y_1)

An in vitro dissolution profile for B1-B9 batches is shown in Fig. 5. The time required for 85% release of a drug from a formulation (t_{85}) is a crucial parameter in evaluating its quality. The effects of the amount of PEG 4000 (X_1)

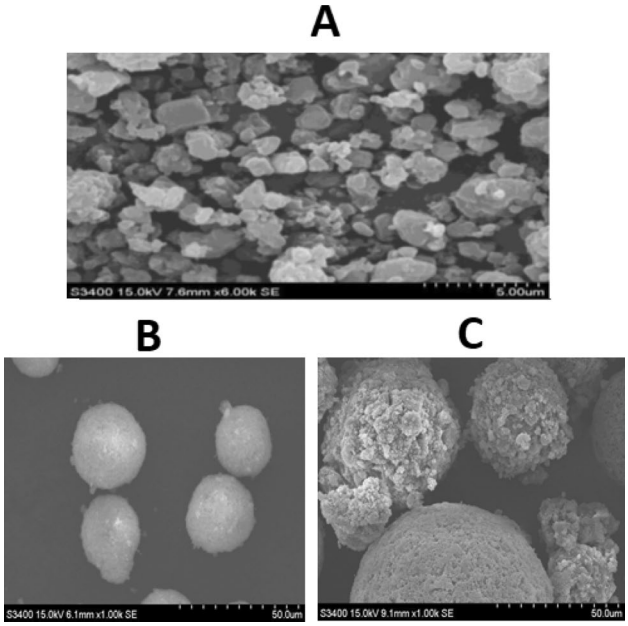

Fig. 4 Scanning electron microscopy image of RXN (**A**), Neusilin US2 (**B**), and RXN SDA (**C**)

and amount of Neusilin US2 (X_2) on t_{85} for RXN-SDA tablets were studied. The t_{85} values for batches B1–B9 were recorded in Table 6 and were found in the range of 8.55–16.10 min.

The lower values of t_{85} for batches B1-B9 in comparison to RXN suspension could be attributed to the molecular dispersion and solubilization of RXN in hydrophilic carrier PEG 4000. Additionally, improved wettability of RXN due to PEG 4000, prevention of drug aggregation and decreased particle size of RXN in SDAs also contribute to lowering of t_{85} (enhanced dissolution rate). Furthermore, reduction in the crystallinity of RXN when dispersed in PEG 4000 in SDAs, is considered a crucial factor in the enhancement of the dissolution rate.

Table 6 Design layouts with respective observed response

Batch no	X_1 amount of carrier	X_2 amount of adsorbent	$Y_1 = t_{85}$ (min)	Y_2 = saturated solubility (g/mL)
B1	−1	−1	16.10	0.026 ± 0.005
B2	−1	0	15.20	0.029 ± 0.001
B3	−1	+1	10.15	0.038 ± 0.006
B4	0	−1	15.30	0.027 ± 0.006
B5	0	0	9.40	0.038 ± 0.003
B6	0	+1	9.10	0.041 ± 0.007
B7	+1	−1	14.45	0.023 ± 0.001
B8	+1	0	9.30	0.028 ± 0.004
B9	+1	+1	8.55	0.031 ± 0.002

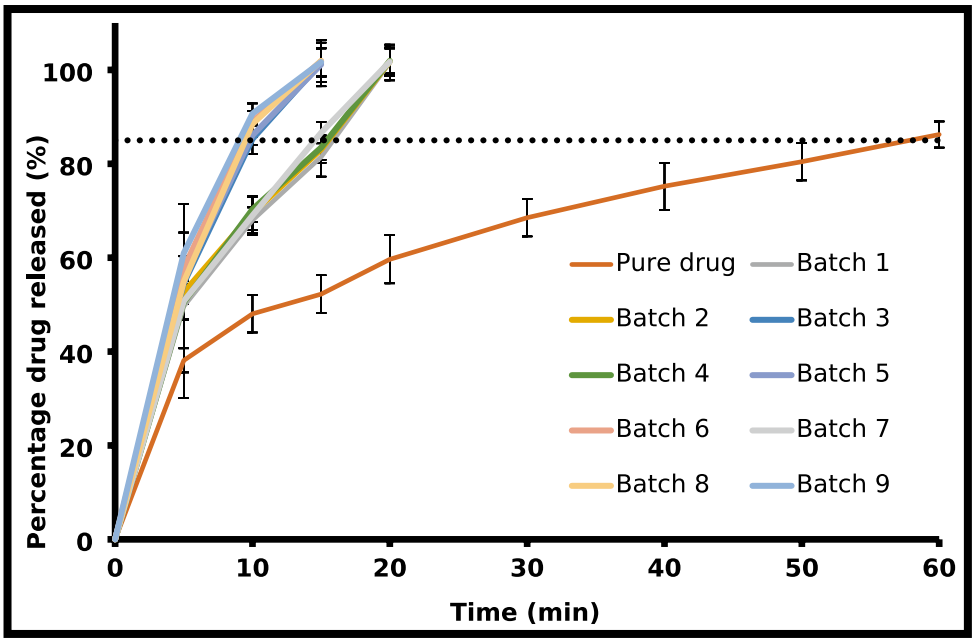

Fig. 5 Comparison of in vitro dissolution profiles of RXN from RXN SDA tablets and pure drug performed in a USP type II tablet dissolution test apparatus. Data presented as the average of six trials ± SD

Neusilin US2, a porous adsorbent, employed in formulating RXN-SDAs possesses an excellent adsorption capacity (3.2 mL/g) and a high specific surface area (300 m^2/g). The adsorption of RXN solid dispersions onto Neusilin US2 in RXN-SDAs would provide an increased effective surface area, which would lead to rapid desorption of the drug upon exposure to dissolution medium [56].

The linear model is selected for this variable. The polynomial equation for Y_1 is as shown below:

$$Y_{1(t85)} = +10.62 - 1.53X_1 - 3.01X_20 \quad (2)$$

The 2D and 3D plots for Y_1 are shown in Fig. 6. From Eq. (2) and Fig. 6, it is clear that X_1 was found to have a negative impact on Y_1. An increase in the amount of PEG 4000 led to a decrease in the time required for 85% drug release. This could be explained as follows: Hydrophilic carrier-PEG 4000 is known to improve the wettability of the drugs [44]. RXN would be present in different proportions of the crystalline and amorphous forms based on the amount of PEG 4000 employed in the preparation of RXN solid dispersion. As the amount of PEG 4000 increases, the amorphous form of RXN is expected to increase, which

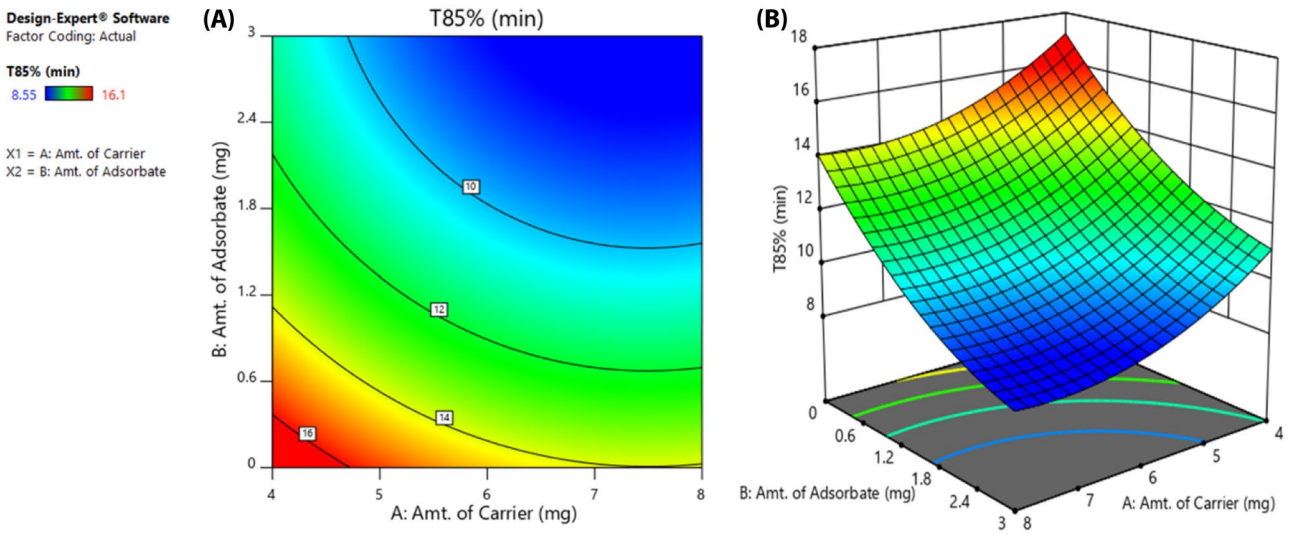

Fig. 6 Contour plot (**A**) and 3D surface plot (**B**) showing the effect of the amount of adsorbent and amount of carrier on time required for 85% drug release

can cause augmentation in the dissolution of RXN and reduction in t_{85}. A similar observation was recorded by our research group while formulating Ticagrelor solid dispersion adsorbates [57]; Kapsi and Ayers [58] while formulating Itraconazole-PEG solid dispersions; Chutimaworapan et al. [59] while formulating Nifedipine solid dispersions in presence of water-soluble carriers like PEG, hydroxyl propyl β-cyclodextrin (HP-β-CD), and poloxamer 407.

As seen from the above equation, the amount of Neusilin US2 (X_2) was also found to have a negative impact on t_{85}. Neusilin US2 provides an enhanced effective surface area [46] leading to the rapid diffusion of RXN into the dissolution medium. The enhanced dissolution rate is suggestive of a reduced t_{85}.

Effect of amount of PEG 4000 (X_1) and amount of Neusilin US2 (X_2) on saturated solubility (Y_2)

Solubility is one of the crucial parameters to achieve the desired concentration of drug in the plasma for anticipated therapeutic response. RXN solubility was found to be 0.012 ± 0.009 g/mL whereas the solubilities for B1-B9 were found to be in the range of 0.023–0.041 g/mL (Table 6). The results indicated that Y_2 is affected by the amount of PEG 4000 and the amount of Neusilin US2. 2D and 3D plots, representing the influence of both independent variables on Y_2 are shown in Fig. 7. The response (Y_2) obtained for two independent variables was subjected to multiple regression to get a quadratic polynomial equation:

$$Y_2(\textit{saturated solubility}) = +0.0358 - 0.0018X_1 + 0.0057X_2 - 0.0062X_1^2 \quad (3)$$

From Eq. (3) and Fig. 7, it is evident that Neusilin US2 has a positive impact on the RXN solubility when SDAs were formulated. An increase in the amounts of Neusilin leads to a linear increment in the solubility. This could be attributed to the increased surface area provided by the novel adsorbent. At constant levels of Neusilin US2, solubility was increased marginally when PEG 4000 was increased from − 1 to 0 levels. This could be due to interaction between PEG 4000 and RXN mainly by electrostatic forces and occasionally by other types of forces like hydrogen bonds [60]. A further increase from 0 to + 1 levels, led to a slight decrease in the solubility.

Optimization and validation overlay and checkpoint analysis

The numerical and graphical optimization approaches were employed to obtain RXN-SDAs with desirability functions close to unity. The overlay plot is shown in Fig. 8, which helps to obtain acceptable fields for the independent variables. The yellow area in the overlay plot exhibits the required design space within which the anticipated results for the responses can be obtained. An optimized formulation with X_1 and X_2 values of 5.7 g and 2.52 g respectively was chosen. The anticipated Y_1 and Y_2 values were 9.27 min. and 0.0395 g/mL respectively. To check the validity of the optimization process, an optimized batch was formulated with the chosen levels of X_1 and X_2. The composition of the optimized RXN SDA tablets is shown in Table 7. The predicted and experimental values of the responses (Y_1 and Y_2) are tabulated in Table 8. The differences between expected and observed values were negligible. The RSM model's validity was verified by the strong agreement between the predicted and experimental values.

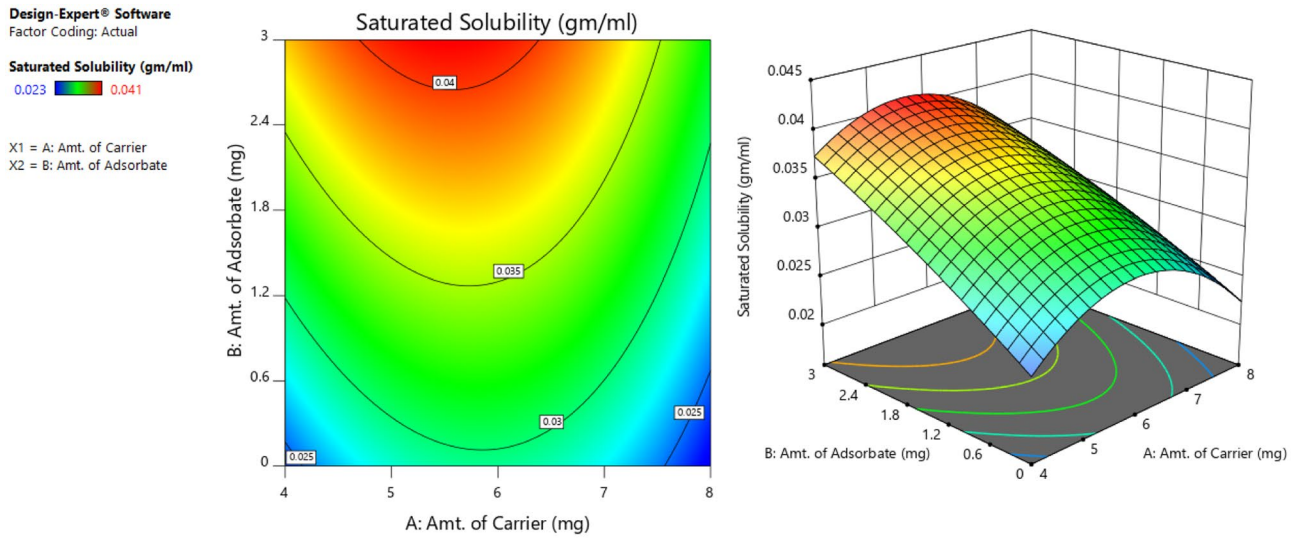

Fig. 7 Contour plot (**A**) and 3D surface plot (**B**) showing the effect of the amount of adsorbent and amount of carrier on saturated solubility

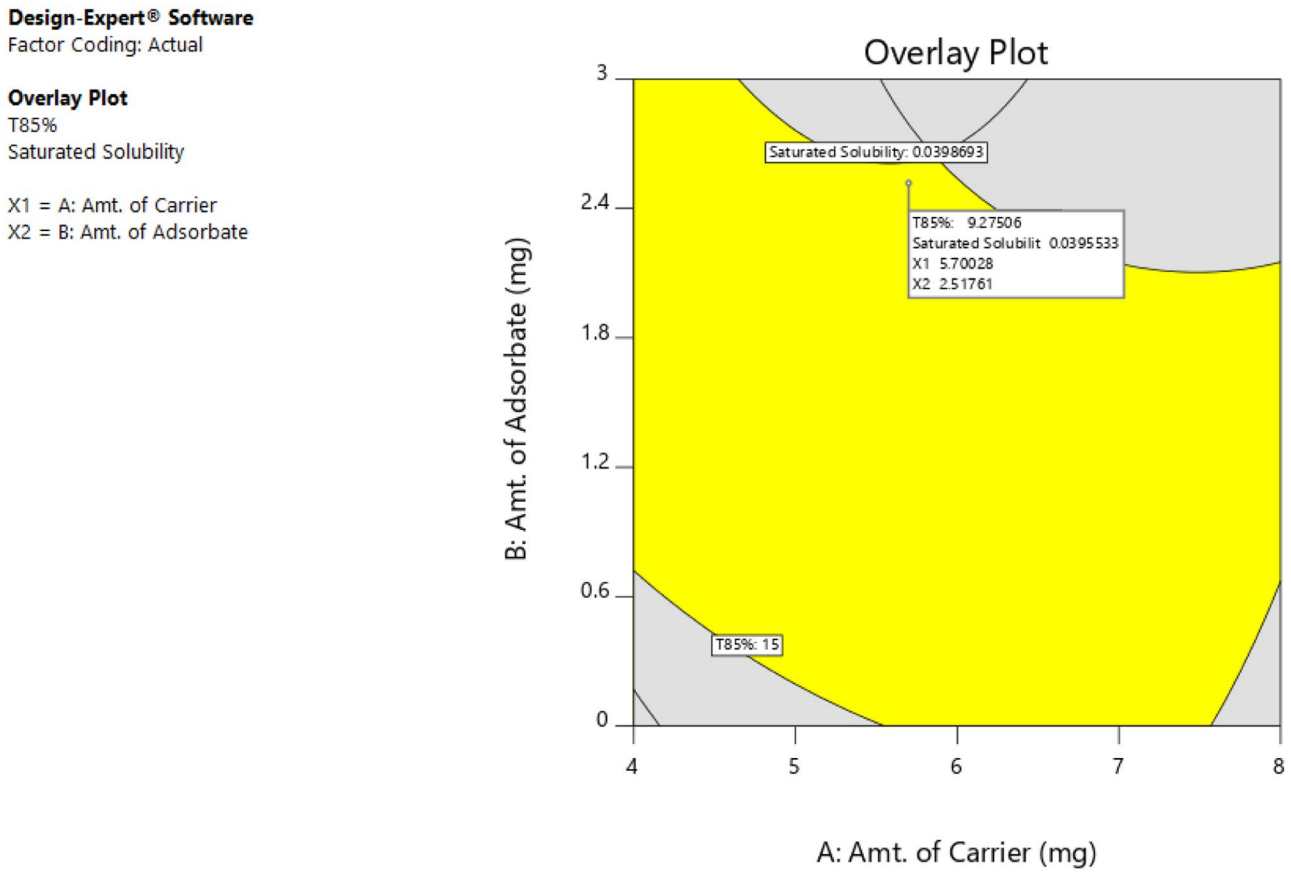

Fig. 8 Overlay plot of the factors and responses

Evaluation of optimized SDA

Pre-compression parameters

The optimized RXN-SDAs were evaluated for flowability and compressibility. The values for the angle of repose, Carr's index, and Hausner's ratio were found to be 17.25 ± 0.29°, 9.20 ± 0.65%, and 1.17 ± 0.08 respectively. The values are suggestive of excellent flowability and compressibility, which would suffice the requirements of scale-up and commercial manufacturing. The saturated solubility of RXN-SDAs was found to be 0.041 ± 0.0007 mg/mL, which is 3.42 folds higher than the pure RXN.

Post-compression parameters

The optimized SDA tablet had been evaluated for its average weight (300 ± 2.97 mg), drug content (98.39 ± 1.2%), thickness (3.44 ± 0.01 mm), hardness (2.41 ± 0.4 kg/cm^2), friability (0.32 ± 0.02%) and disintegration time (26 ± 2.64 s). All the parameters were in the acceptable range.

Table 7 Formulation table of the optimized batch of RXN SDA tablets

Ingredients	Quantity (mg)
Solid dispersion adsorbate*	216
Crospovidone	15
Micro crystalline cellulose	64
Talc	2.5
Magnesium stearate	2.5
Total weight	**300 mg**

*Equivalent to 10 mg of rivaroxaban

Table 8 Composition of check point batch along with predicted and observed values

X_1 (g)	X_2 (g)	Parameters	t_{85} (min)	Saturated solubility (g/mL)
5.7	2.517	Observed value	9.55	0.041 ± 0.0007
		Predicted value	9.275	0.039

In vitro dissolution

In vitro release of pure RXN, RXN-SDA tablets, marketed tablets (Xarelto® 10 mg), and directly compressible tablets were carried out using USP type-II apparatus. The release profile is represented in Fig. 9. The t_{85} for pure RXN, RXN-SDA tablets, marketed tablets, and directly compressible tablets were found to be 59.13 min, 9.55 min, 20.16 min, and 19.22 min. The highest value of t_{85} for RXN suspension could be attributed to its poor aqueous solubility and crystalline nature. t_{85} for directly compressible tablets were significantly ($P < 0.05$) lower than the value for RXN suspension, which could be attributed to improved wetting due to the presence of hydrophilic carrier PEG 4000. t_{85} for marketed tablets were significantly ($P < 0.05$) lower than the value for pure RXN, which could be attributed to the presence of hypromellose, sodium lauryl sulfate, and croscarmellose sodium [61]. Furthermore, RXN-SDA tablets exhibited the lowest t_{85} values in comparison to pure RXN, marketed tablets, and directly compressible tablets. The rapid dissolution rate of RXN-SDA tablets is due to the molecular dispersion of RXN in PEG 4000, which leads to amorphization of the drug. Furthermore, the adsorption of RXN-SDAs onto Neusilin US2 provides a higher surface area enabling improved dissolution.

Our developed formulation (RXN-SDA tablets) exhibited a higher rate and extent of dissolution at all the time points in comparison to the Xarelto tablets. The higher in vitro dissolution, attributable to a multitude of mechanisms described above, could be the causative reason for augmented in vivo dissolution. Higher in vivo dissolution might, in turn, provide a faster T_{max} and a higher C_{max}, AUC, and bioavailability along with reduced dose, side-effects, cost of therapy, better patient compliance, and improved management of hypertension.

Cytotoxicity test

To evaluate the cytotoxic effect of RXN SDA tablet and RXN suspension, an MTT assay was performed on Caco-2 cells [62, 63]. The untreated cells exhibited 100% cell viability. The cell viabilities associated with 20vμM, 40-μM, 60-μM, 80-μM, and 100-μM RXN suspension were found to be 99.41%, 99.24%, 99.74%, 97.89%, and 95.58% respectively. The corresponding values associated with RXN SDA tablets were 99.35%, 98.85%, 98.63%, 97.47%, and 96.54% respectively. No significant difference was observed in the cell viabilities of both the formulations Even, the highest concentration (100 μM) of the RXN SDA tablet exhibited a > 95% cell viability indicating the absence of cytotoxicity.

Pharmacokinetic study

Based on the plasma concentration–time profile (Fig. 10), corresponding pharmacokinetic parameters were determined and tabulated in Table 9. The T_{max} for RXN SDA tablets and Xarelto tablets were 2 h, whereas the value for RXN suspension was 3 h. The faster absorption of RXN SDA tablets and Xarelto tablets relative to RXN suspension could likely

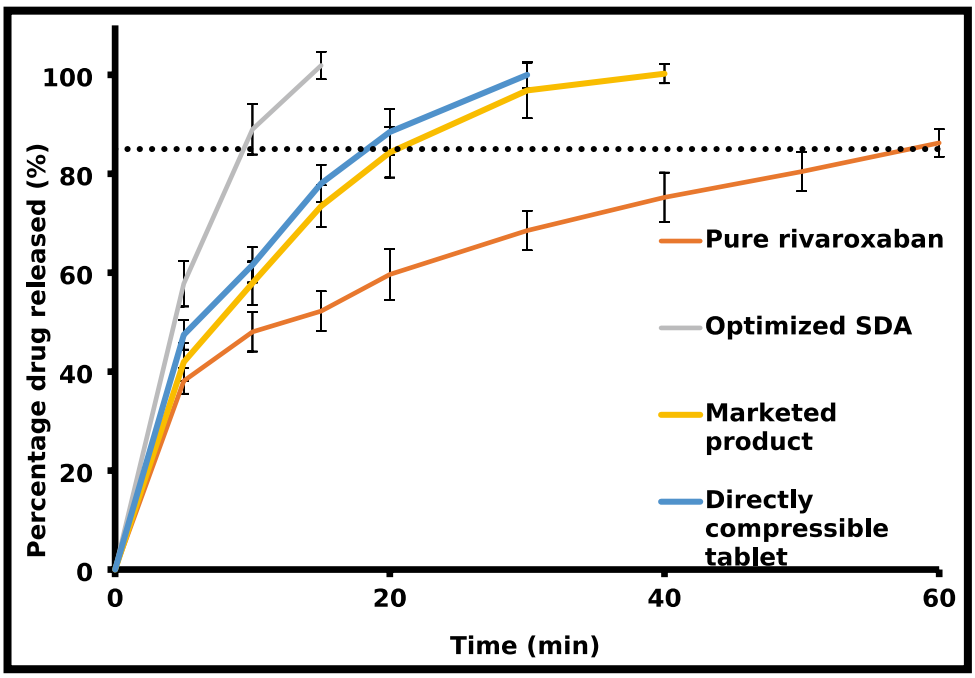

Fig. 9 Comparison of in vitro dissolution profiles of RXN, RXN SDA tablets, marketed tablets product, and directly compressible tablets performed in USP type II tablet dissolution test apparatus. Data presented as the average of six trials ± SD

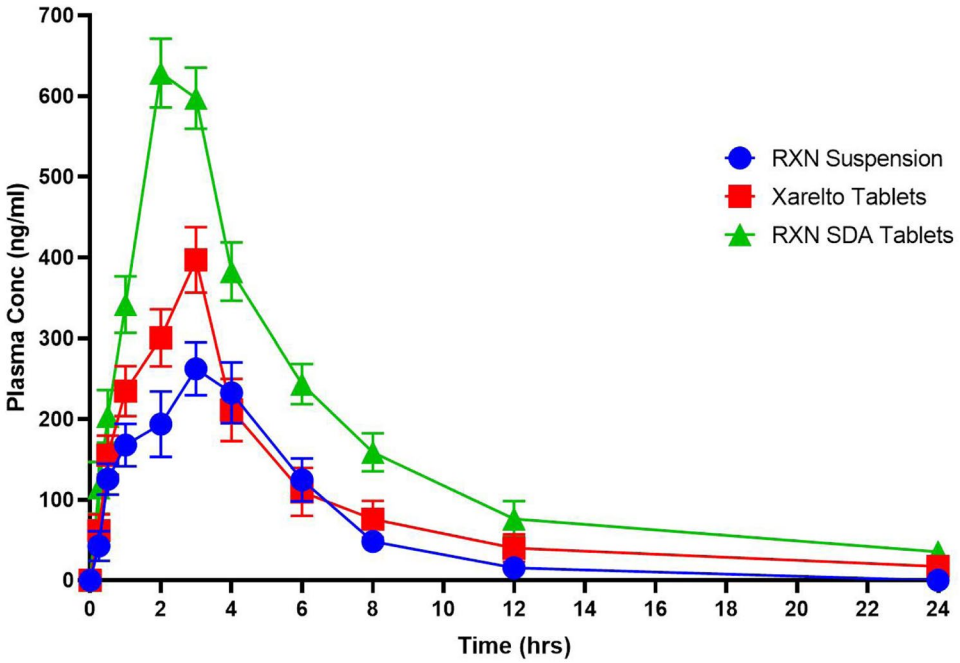

Fig. 10 Plasma concentration vs. time curve of RXN from RXN suspension, Xarelto tablets, and RXN SDA tablets

provide a quicker onset of action which could be attributed to the increase in dissolution rate and solubility of RXN from the SDA tablets and Xarelto tablets in the gastrointestinal tract, allowing rapid absorption of the drug. The C_{max} values for RXN suspension, RXN SDA tablets, and Xarelto tablets were found to be 262.32 ± 32.71 ng/mL, 628.83 ± 42.60 ng/mL, and 397.16 ± 40.54 ng/mL respectively. The C_{max} values for RXN SDA tablets were 2.4 times and 1.58 times higher than RXN suspension and Xarelto tablets respectively indicating the ability of the developed formulation in providing higher levels of RXN in plasma. The $AUC_{0–24}$ values for RXN suspension, RXN SDA tablets and Xarelto tablets were found to be 1414.09 ± 192.18 ng.h/mL, 3945.37 ± 300.71 ng.h/mL and 2136.65 ± 153.86 ng.h/mL respectively. The $AUC_{0–24}$ values achieved with RXN SDA tablets were 2.79- and 1.85-fold higher in comparison to RXN suspension and Xarelto tablets respectively (Table 9). The results of this study are in-line with the in vitro release studies. These values clearly indicated augmentation in bioavailability of RXN from SDAs when compared to its suspension and marketed formulation, confirming an increase in solubility and dissolution rate thus enhancing the oral bioabsorption. A similar observation was noticed in earlier studies with other drugs as well [64]. The outcomes of this study may be extrapolated towards the possibilities of dose reduction upon the administration of the test formulation. Literature suggests that food does not affect the AUC or C_{max} when a 10-mg oral dose is administered [2]. However, for higher doses (20 mg), the fed state exhibits improved bioavailability. Hence, the food intake along with the fold in solubility improvement has to be jointly considered for dose escalation studies.

Pharmacodynamic studies

Tail bleeding time assay

To discern the antithrombotic and associated antihemostatic effects of 0.5% CMC (control), RXN suspension,

Table 9 Pharmacokinetic parameters for rivaroxaban formulations after administration in Sprague–Dawley rats

Parameters	RXN SUSP	RXN SDA tablets	Xarelto tablets
T_{max} (h)	3.0	2.0	3.0
C_{max} (ng/mL)	262.32 ± 32.71	628.83 ± 42.60	397.16 ± 40.54
$AUC_{0–24}$ (ng.h/mL)	1414.09 ± 192.18	3945.37 ± 300.71	2136.65 ± 153.86
$AUC_{0–\infty}$ (ng.h/mL)	1462.00 ± 207.35	4257.14 ± 311.15	2314.36 ± 166.55
Relative bioavailability	–	279% compared to RXN SUSP 185% compared to Xarelto tablets	151% compared to RXN SUSP 54% compared to RXN SDA tablets

and RXN SDA tablets; bleeding time was investigated in the rat tail model. The bleeding times recorded with control, RXN suspension, and RXN SDA tablets were found to be 68.00 ± 9.08 s, 126.00 ± 6.52 s, and 189.00 ± 7.70 s respectively. RXN SDA tablets exhibited significantly higher ($P < 0.05$) prolongation of bleeding time in comparison to control and RXN suspension. The higher efficacy of the developed formulation along with the reversible binding of RXN to Factor Xa would probably provide greater clinical benefits compared to other antiplatelet agents.

Platelet aggregation

The effects of various formulations [0.5% CMC (control), RXN suspension, and RXN SDA tablets] on collagen-induced platelet aggregation were evaluated 4 h post-dosing. The Control group exhibited a value of 55.62 ± 2.95% whereas the values exhibited by RXN suspension and RXN SDA tablets were 24.37 ± 1.86% and 13.78 ± 1.62%, respectively. The highest reduction in percentage platelet aggregation registered by RXN SDA tablets can be ascribed to the improved bioavailability of RXN, which ultimately inhibits Factor Xa leading to potentiation of the antiplatelet action. The data are in agreement with pharmacokinetic studies asserting the clinical benefit of the developed novel formulation of RXN. A similar finding has been reported by another research group [65].

Conclusion

This work demonstrated the amalgamation of solid dispersion and melt adsorption technologies in formulating RXN-SDAs, wherein the ternary system comprised of RXN (insoluble drug), PEG 4000 (hydrophilic carrier), and Neusilin US2 (high surface area adsorbent). A DoE approach was employed in the optimization of RXN-SDAs. RXN-SDA blends exhibited better flow properties and higher solubility as compared to pure drugs. RXN-SDA tablets exhibited a lower t_{85} in comparison to the pure drug, marketed tablets, and directly compressible tablets. MTT assay confirmed the absence of cytotoxicity in the developed formulation. RXN-SDA tablets exhibited improved bioavailability and rapid onset of action in comparison to the pure drug and marketed formulation when evaluated in a rodent model. Similarly, bleeding time and platelet aggregation studies suggested superior anticoagulant efficacy of RXN-SDA tablets in comparison to a pure drug. The improved bioabsorption would provide a reduction in dose, dose-related side effects, cost of therapy, and better patient compliance. The studies are proof of the concept that RXN-SDAs prepared by this simple, economic, scalable, and solvent-free process can prove to be a viable alternative in the management of stroke and embolism. However, scale-up, validation, and clinical studies are required for the successful translation of this dosage form from bench to bedside.

Supplementary information The online version contains supplementary material available at https://doi.org/10.1007/s13346-022-01168-9.

Acknowledgements The authors acknowledge the management of Maliba Pharmacy College, Bardoli, Surat, India for the support.

Author contribution Pranav J. Shah: Conceptualization, data curation, formal analysis, investigation, methodology, writing—review and editing. Patel Milan Pankajkumar: Conceptualization, data curation, formal analysis, investigation, methodology, writing—original draft preparation. Jigar Shah: Formal analysis, investigation, methodology, writing—review and editing. Sabna Kotta: Formal analysis, investigation, methodology, writing—review and editing. Anroop B. Nair: Formal analysis, investigation, methodology, writing—review and editing. Bhavin Vyas: Pharmacokinetic and pharmacodynamic studies, writing—review and editing.

Funding The funding for the research work was provided by Maliba Pharmacy College.

Data availability All the data related to the manuscript has been included. The materials used in the experiments have been included in the "Materials and methods" section.

Declarations

Ethics approval and consent to participate All institutional and national guidelines for the care and use of laboratory animals were followed.

Consent for publication All authors have read and provided consent for the publication of the manuscript.

Competing interests The authors declare no competing interests.

References

1. Mueck W, Stampfuss J, Kubitza D, Becka M. Clinical Pharmacokinetic and pharmacodynamic profile of rivaroxaban. Clin Pharmacokinet. 2014;53(1):1–16.
2. Abouhussein DMN, Bahaa El Din Mahmoud D, Mohammad FE. Design of a liquid nano-sized drug delivery system with enhanced solubility of rivaroxaban for venous thromboembolism management in paediatric patients and emergency cases. J Liposome Res. 2019;29(4):399–412.
3. Xue X, Cao M, Ren L, Qian Y, Chen G. Preparation and optimization of rivaroxaban by self-nanoemulsifying drug delivery system (SNEDDS) for enhanced oral bioavailability and no food effect. AAPS PharmSciTech. 2018;19(4):1847–59.
4. Anwer MK, Mohammad M, Iqbal M, Ansari MN, Ezzeldin E, Fatima F, et al. Sustained release and enhanced oral bioavailability of rivaroxaban by PLGA nanoparticles with no food effect. J Thromb Thrombolysis. 2020;49(3):404–12.
5. Zhang X, Xing H, Zhao Y, Ma Z. Pharmaceutical dispersion techniques for dissolution and bioavailability enhancement of poorly water-soluble drugs. Pharmaceutics. 2018;10(3). https://doi.org/10.3390/pharmaceutics10030074.

6. Sree Harsha N, Hiremath JG, Sarudkar S, Attimarad M, Al-Dhubiab B, Nair AB, et al. Spray dried amorphous form of simvastatin: preparation and evaluation of the buccal tablet. Indian Journal of Pharmaceutical Education and Research. 2020;54:46–54.
7. Jacob S, Nair AB, Shah J. Emerging role of nanosuspensions in drug delivery systems. Biomaterials research. 2020;24(1):1–16.
8. Jacob S, Nair AB. Cyclodextrin complexes: Perspective from drug delivery and formulation. Drug Dev Res. 2018;79(5):201–17.
9. Sherje AP, Jadhav M. β-Cyclodextrin-based inclusion complexes and nanocomposites of rivaroxaban for solubility enhancement. J Mater Sci - Mater Med. 2018;29(12):186. https://doi.org/10.1007/s10856-018-6194-6.
10. Chen N, Di P, Ning S, Jiang W, Jing Q, Ren G, et al. Modified rivaroxaban microparticles for solid state properties improvement based on drug-protein/polymer supramolecular interactions. Powder Technol. 2019;344:819–29.
11. Nepal PR, Han HK, Choi HK. Enhancement of solubility and dissolution of coenzyme Q10 using solid dispersion formulation. Int J Pharm. 2010;383(1–2):147–53.
12. Craig DQ. The mechanisms of drug release from solid dispersions in water-soluble polymers. Int J Pharm. 2002;231(2):131–44.
13. Kapourani A, Eleftheriadou K, Kontogiannopoulos KN, Barmpalexis P. Evaluation of rivaroxaban amorphous solid dispersions physical stability via molecular mobility studies and molecular simulations. Eur J Pharm Sci. 2021;157: 105642. https://doi.org/10.1016/j.ejps.2020.105642.
14. Metre S, Mukesh S, Samal SK, Chand M, Sangamwar AT. Enhanced biopharmaceutical performance of rivaroxaban through polymeric amorphous solid dispersion. Mol Pharm. 2018;15(2):652–68.
15. Ganesh M, Shekar BC, Madhusudan Y . Design and optimization of rivaroxaban lipid solid dispersion for dissolution enhancement using statistical experimental design. Asian Journal of Pharmaceutics (AJP): Free full text articles from Asian J Pharm. 2016;10(1)59–64.
16. Alshehri S, Imam SS, Hussain A, Altamimi MA, Alruwaili NK, Alotaibi F, Alanazi A, Shakeel F. Potential of solid dispersions to enhance solubility, bioavailability, and therapeutic efficacy of poorly water-soluble drugs: newer formulation techniques, current marketed scenario and patents. Drug Delivery. 2020;27(1):1625–43.
17. Mahajan A, Surti N, Koladiya P. Solid dispersion adsorbate technique for improved dissolution and flow properties of lurasidone hydrochloride: characterization using 3(2) factorial design. Drug Dev Ind Pharm. 2018;44(3):463–71.
18. Kaushik D, Singh N, Arora A. Enhancement of dissolution profile of gliclazide by solid dispersion adsorbates. Lat Am J Pharm. 2011;30:2057–60.
19. Gupta MK, Goldman D, Bogner RH, Tseng YC. Enhanced drug dissolution and bulk properties of solid dispersions granulated with a surface adsorbent. Pharm Dev Technol. 2001;6(4):563–72.
20. Hentzschel CM, Alnaief M, Smirnova I, Sakmann A, Leopold CS. Tableting properties of silica aerogel and other silicates. Drug Dev Ind Pharm. 2012;38(4):462–7.
21. Wang Y, Zhao Q, Hu Y, Sun L, Bai L, Jiang T, Wang S. Ordered nanoporous silica as carriers for improved delivery of water insoluble drugs: a comparative study between three dimensional and two dimensional macroporous silica. Int J Nanomed. 2013;8:4015–31.
22. Tawfeek HM, Roberts M, El Hamd MA, Abdellatif AAH, Younis MA. Glibenclamide mini-tablets with an enhanced pharmacokinetic and pharmacodynamic performance. AAPS PharmSciTech. 2018;19(7):2948–60.
23. Nair AB, Chakraborty B, Murthy SN. Effect of polyethylene glycols on the trans-ungual delivery of terbinafine. Curr Drug Deliv. 2010;7(5):407–14.
24. Shah J, Vasanti S, Anroop B, Vyas H. Enhancement of dissolution rate of valdecoxib by solid dispersions technique with PVP K 30 & PEG 4000: preparation and in vitro evaluation. J Incl Phenom Macrocycl Chem. 2009;63(1):69–75.
25. Altamimi MA, Elzayat EM, Qamar W, Alshehri SM, Sherif AY, Haq N, Shakeel F. Evaluation of the bioavailability of hydrocortisone when prepared as solid dispersion. Saudi pharmaceutical journal. 2019;27(5):629–36.
26. Farmoudeh A, Rezaeiroshan A, Abbaspour M, Nokhodchi A, Ebrahimnejad P. Solid dispersion pellets: an efficient pharmaceutical approach to enrich the solubility and dissolution rate of deferasirox. Biomed Res Int. 2020;2020:8583540. https://doi.org/10.1155/2020/8583540.
27. Raval MK, Patel JM, Parikh RK, Sheth NR. Dissolution enhancement of chlorzoxazone using cogrinding technique. International journal of pharmaceutical investigation. 2015;5(4):247–58.
28. Jhaveri M, Nair AB, Shah J, Jacob S, Patel V, Mehta T. Improvement of oral bioavailability of carvedilol by liquisolid compact: optimization and pharmacokinetic study. Drug Deliv Transl Res. 2020;10(4):975–85.
29. Kwon J, Giri BR, Song ES, Bae J, Lee J, Kim DW. Spray-dried amorphous solid dispersions of atorvastatin calcium for improved supersaturation and oral bioavailability. Pharmaceutics. 2019;11(9):461. https://doi.org/10.3390/pharmaceutics11090461.
30. Nair A, Gupta R, Vasanti S. In vitro controlled release of alfuzosin hydrochloride using HPMC-based matrix tablets and its comparison with marketed product. Pharm Dev Technol. 2007;12(6):621–5.
31. Harsha SN, Aldhubiab BE, Nair AB, Alhaider IA, Attimarad M, Venugopala KN, Srinivasan S, Gangadhar N, Asif AH. Nanoparticle formulation by Büchi B-90 nano spray dryer for oral mucoadhesion. Drug Des Dev Ther. 2015;9:273–82.
32. Sakure K, Kumari L, Badwaik H. Development and evaluation of solid dispersion based rapid disintegrating tablets of poorly water-soluble anti-diabetic drug. J Drug Delivery Sci Technol. 2020;60:101942. https://doi.org/10.1016/j.jddst.2020.101942.
33. Çelebier M, Kaynak M, Altinoz S, Selma S. UV spectrophotometric method for determination of the dissolution profile of rivaroxaban. Dissolut Technol. 2014;21:56–9.
34. Abdallah MA, Al-Ghobashy MA, Lotfy HM. Investigation of the profile and kinetics of degradation of rivaroxaban using HPLC, TLC-densitometry and LC/MS/MS: application to pre-formulation studies. Bulletin of Faculty of Pharmacy, Cairo University. 2015;53(1):53–61.
35. Shah P, Sarolia J, Vyas B, Wagh P, Kaul A, Mishra AK. PLGA nanoparticles for nose to brain delivery of clonazepam: formulation, optimization by 3^2 factorial design, in-vitro and in-vivo evaluation. Curr Drug Deliv. 2021;18(6):805–24.
36. Borderwala K, Swain G, Mange N, Gandhi J, Lalan M, Singhvi G, Shah P. Optimization of solid lipid nanoparticles of ezetimibe in combination with simvastatin using quality by design (QbD). Nanoscience & Nanotechnology-Asia. 2020;10(4):404–18.
37. Naik B, Gandhi J, Shah P, Naik H, Sarolia J. Asenapine maleate loaded solid lipid nanoparticles for oral delivery. International Research Journal of Pharmacy. 2017;8:45–53.
38. Nair AB, Al-Dhubiab BE, Shah J, Jacob S, Saraiya V, Attimarad M, SreeHarsha N, Akrawi SH, Shehata TM. Mucoadhesive buccal film of almotriptan improved therapeutic delivery in rabbit model. Saudi pharmaceutical journal. 2020;28(2):201–9.
39. Nair AB, Sreeharsha N, Al-Dhubiab BE, Hiremath JG, Shinu P, Attimarad M, Venugopala KN, Mutahar M. HPMC- and PLGA-based nanoparticles for the mucoadhesive delivery of sitagliptin: optimization and in vivo evaluation in rats. Materials. 2019;12:4239. https://doi.org/10.3390/ma12244239.

40. Nair AB, Al-Dhubiab BE, Shah J, Attimarad M, Harsha S. Poly (lactic acid-co-glycolic acid) Nanospheres improved the oral delivery of candesartan cilexetil. Indian J Pharm Educ Res. 2017;51:571–9.
41. Akrawi SH, Gorain B, Nair AB, Choudhury H, Pandey M, Shah JN, Venugopala KN. Development and optimization of naringenin-loaded chitosan-coated nanoemulsion for topical therapy in wound healing. Pharmaceutics. 2020;12(9):893. https://doi.org/10.3390/pharmaceutics12090893.
42. Chong J, Chen H, Dai D, Wang S, Zhou Q, Liu J, et al. Effects of ticagrelor on the pharmacokinetics of rivaroxaban in rats. Pharm Biol. 2020;58(1):630–5.
43. Chaudhary S, Nair AB, Shah J, Gorain B, Jacob S, Shah H, Patel V. Enhanced solubility and bioavailability of dolutegravir by solid dispersion method: in vitro and in vivo evaluation—a potential approach for HIV therapy. AAPS PharmSciTech. 2021;22(3):127. https://doi.org/10.1208/s12249-021-01995-y.
44. Zhang WL, Lou D, Zhang DT, Zhang Y, Huang HJ. Determination of rivaroxaban, apixaban and edoxaban in rat plasma by UPLC-MS/MS method. J Thromb Thrombolysis. 2016;42(2):205–11.
45. Nair A, Morsy MA, Jacob S. Dose translation between laboratory animals and human in preclinical and clinical phases of drug development. Drug Dev Res. 2018;79(8):373–82.
46. Wang YY, Tang ZY, Dong M, Liu XY, Peng SQ. Inhibition of platelet aggregation by polyaspartoyl L-arginine and its mechanism. Acta Pharmacol Sin. 2004;25(4):469–73.
47. Mekhfi H, El Haouari M, Legssyer A, Bnouham M, Aziz M, Atmani F, et al. Platelet anti-aggregant property of some Moroccan medicinal plants. J Ethnopharmacol. 2004;94(2–3):317–22.
48. Born GV. Aggregation of blood platelets by adenosine diphosphate and its reversal. Nature. 1962;194:927–9.
49. Liu Y, Wang T, Ding W, Dong C, Wang X, Chen J, Li Y. Dissolution and oral bioavailability enhancement of praziquantel by solid dispersions. Drug Deliv Transl Res. 2018;8(3):580–90.
50. Vojinović T, Medarević D, Vranić E, Potpara Z, Krstić M, Djuriš J, Ibrić S. Development of ternary solid dispersions with hydrophilic polymer and surface adsorbent for improving dissolution rate of carbamazepine. Saudi pharmaceutical journal. 2018;26(5):725–32.
51. Sruti J, Patra ChN, Swain SK, Beg S, Palatasingh HR, Dinda SC, BhanojiRao ME. Improvement in dissolution rate of cefuroxime axetil by using Poloxamer 188 and Neusilin US2. Indian J Pharm Sci. 2013;75(1):67–75.
52. Tafu NN, Jideani VA. Characterization of novel solid dispersions of Moringa oleifera leaf powder using thermo-analytical techniques. Processes. 2021;9:2230. https://doi.org/10.3390/pr9122230.
53. Taokaew S, Ofuchi M, Kobayashi T. Chitin biomass-nifedipine amorphous solid dispersion for enhancement of hydrophobic drug dissolution in aqueous media. Sustain Chem Pharm. 2020;17:100284. https://doi.org/10.1016/j.scp.2020.100284.
54. Lee HJ, Kim JY, Park SH, Rhee YS, Park CW, Park ES. Controlled-release oral dosage forms containing nimodipine solid dispersion and hydrophilic carriers. J Drug Deliv Sci Technol. 2017;37:28–37.
55. Komínová P, Kulaviak L, Zámostný P. Stress-dependent particle interactions of magnesium aluminometasilicates as their performance factor in powder flow and compaction applications. Materials. 2021;14(4):900. https://doi.org/10.3390/ma14040900.
56. Gupta MK, Goldman D, Bogner RH, Tseng YC. Enhanced drug dissolution and bulk properties of solid dispersions granulated with a surface adsorbent. Pharm Dev Technol. 2001;6:563–72.
57. Yadav M, Sarolia J, Vyas B, Lalan M, Mangrulkar S, Shah P. Amalgamation of solid dispersion and melt adsorption technique: improved in vitro and in vivo performance of ticagrelor tablets. AAPS PharmSciTech. 2021;22(8):257. https://doi.org/10.1208/s12249-021-02138-z.
58. Kapsi SG, Ayres JW. Processing factors in development of solid solution formulation of itraconazole for enhancement of drug dissolution and bioavailability. Int J Pharm. 2001;229:193–203.
59. Chutimaworapan S, Ritthidej GC, Yonemochi E, et al. Effect of water-soluble carriers on dissolution characteristics of nifedipine solid dispersions. Drug Dev Ind Pharm. 2000;26:1141–50.
60. Balata G, Mahdi M, Bakera RA. Improvement of solubility and dissolution properties of clotrimazole by solid dispersions and inclusion complexes. Indian J Pharm Sci. 2011;73(5):517–26.
61. https://www.rxlist.com/xarelto-drug.htm#description. Accessed 9 Dec 2021.
62. da Silva LC, Garcia T, Mori M, Sandri G, Bonferoni MC, Finotelli PV, Cinelli LP, Caramella C, Cabral LM. Preparation and characterization of polysaccharide-based nanoparticles with anticoagulant activity. Int J Nanomedicine. 2012;7:2975–86.
63. Patel M, Mundada V, Sawant K. Enhanced intestinal absorption of asenapine maleate by fabricating solid lipid nanoparticles using TPGS: elucidation of transport mechanism, permeability across Caco-2 cell line and in vivo pharmacokinetic studies. Artificial Cells, Nanomedicine, and Biotechnology. 2019;47(1):144–53.
64. Kim SJ, Lee HK, Na YG, Bang KH, Lee HJ, Wang M, et al. A novel composition of ticagrelor by solid dispersion technique for increasing solubility and intestinal permeability. Int J Pharm. 2019;555:11–8.
65. Perzborn E, Heitmeier S, Laux V. Effects of rivaroxaban on platelet activation and platelet-coagulation pathway interaction: in vitro and in vivo studies. J Cardiovasc Pharmacol Ther. 2015;20(6):554–62.